Inherent spin–polarization coupling in a magnetoelectric vortex

Sujit Das,*[$1] Valentyn Laguta,*[2] Katherine Inzani,*[3,4,5] Weichuan Huang,[6] Junjie Liu,[7] Ruchira Chatterjee,[3] Margaret R. McCarter,[8] Sandhya Susarla,[3] Arzhang Ardavan,[7] Javier Junquera,[9] Sinéad M. Griffin,[3,4] and Ramamoorthy Ramesh[3,6,8]

[1] Material Research Centre, Indian Institute of Science, Bangalore, 560012, India

[2] Institute of Physics of the Czech Academy of Sciences, Cukrovarnická 10, 162 00 Prague, Czech Republic

[3] Materials Sciences Division, Lawrence Berkeley National Laboratory, Berkeley, California 94720, USA

[4] Molecular Foundry, Lawrence Berkeley National Laboratory, Berkeley, California 94720, USA

[5] School of Chemistry, University of Nottingham, University Park, Nottingham, NG7 2RD, United Kingdom

[6] Department of Materials Science and Engineering, University of California, Berkeley, California 94720, USA

[7] CAESR, Department of Physics, University of Oxford, The Clarendon Laboratory, Parks Road, Oxford OX1 3PU, United Kingdom

[8] Department of Physics, University of California, Berkeley, California 94720, USA

[9] Departamento de Ciencias de la Tierra y Física de la Materia Condensada, Universidad de Cantabria, Cantabria Campus Internacional, Avenida de los Castros s/n, E-39005 Santander, Spain

(* authors contributed equally to this work)

[$]Corresponding author's email: sujitdas@iisc.ac.in

Solid-state materials are currently being explored as a platform for the manipulation of spins for spintronics and quantum information science. More broadly, a wide spectrum of ferroelectric materials, spanning inorganic oxides to polymeric systems such as PVDF present a different approach to explore quantum phenomena in which the spins are set and manipulated with electric fields. Using dilute Fe^{3+}-doped ferroelectric $PbTiO_3$-$SrTiO_3$ superlattices as a model system, we demonstrate intrinsic spin-polarization control of spin directionality in complex ferroelectric vortices and skyrmions. Electron paramagnetic resonance (EPR) spectra show that the spins in the Fe^{3+} ion are strongly coupled to the local polarization and preferentially aligned perpendicular to the ferroelectric polar *c*-axis in this complex vortex structure. The effect of polarization-spin directionality is corroborated by first-principles calculations, demonstrating the variation of the spin directionality with the polar texture and offering the potential for future quantum analogs of macroscopic magneto-electric devices.

Materials which exhibit coupling between magnetic and electric degrees of freedom are an important class of multifunctional materials. Based on the fascinating fundamental materials physics of spin-charge coupling, such materials present opportunities for future computing.[1,2] Much interest is currently focused on insulating multiferroic and magnetoelectrics, where one is able to switch the magnetization by an *E*-field, thus providing a pathway for low power spintronics.[3,4,5,6,7,8,9,10] All these approaches are directed at the manipulation of the macroscopic magnetic order by applied fields. However, manipulating a single spin via an electric field has possible importance in spin-based nanoelectronics. Previously, such control over individual spins and the tuning of magnetic exchange with electric fields was achieved in molecular systems and semiconductors.[11,12,13,14] Within this framework, perovskite complex oxides provide a highly tunable platform to explore novel physical phenomena and exotic phases arising from the interplay between spin, charge, orbital, and lattice degrees of freedom.[15,16] In particular, ferroelectric oxides in thin film form have been shown to further expand the range of interesting phenomena that can be achieved with the application of relatively low voltages due to the strong role of epitaxial strain in modulating the polar state.[17] This is especially true in ferroelectric materials where the appropriate choice of constituents leads to structures with complex phase diagrams and rich physics.[18,19,20]

A promising pathway to form isolated spins coupled with polarization is to dope a ion with spins in a ferroelectric host compound in a controlled fashion, for example, Fe^{3+} in $PbTiO_3$.[21] The spin-orbit interactions which couple the orbitals in the Fe^{3+} to the ferroelectric $PbTiO_3$ host are responsible for the material's exotic functionalities. Using this prototypical example, it was shown that the spin easy plane is coupled perpendicularly to the direction of the polar distortion through the spin-orbit interaction; furthermore, this could be manipulated coherently using an electric field.[21] This, in conjunction with discovery of polar textures (vortices and skyrmions

that are the dipolar analogs of magnetic skyrmions) in epitaxial superlattices of ferroelectric $PbTiO_3$ with the nonpolar $SrTiO_3$, provides us with a unique platform to study the interactions of such spins with curling electric dipolar fields.[22,23] A recent study demonstrated that the spatial orientation of the Ti^{4+} *d*-orbitals indeed responds to this curling field.[24] Here we demonstrate the intrinsic coupling of an assembly of isolated impurity spins with the rotational polarization in the ferroelectric host, thus illustrating the atomic scale limit of spin-polarization coupling in a solid-state material with potential implications for spin-based classical and quantum computing. As our model system, we consider a thin film ferroelectric, $PbTiO_3$, with dilute (1%) amounts of cations that carry spin (in this case our dopant is Fe^{3+}, which has a high spin S=5/2, d^5 electronic structure, substituted onto the Ti^{4+} site) which is epitaxially constrained by the non-ferroelectric $SrTiO_3$ to create an superlattice structure [(16 u.c. Fe-$PbTiO_3$/16 u.c. $SrTiO_3$)$_8$ superlattice (with a total thickness of 100 nm)]. Imposing electrostatic and elastic boundary conditions at the heterointerfaces in such a superlattice structure is a key ingredient that leads to the formation of the polar textures.

Electron paramagnetic resonance (EPR) has proven to be invaluable in probing the electronic and magnetic structures of such impurities.[25,26,27] However, to date no work has focused on understanding and manipulating the spin state of such impurities using an *E*-field (also internal local fields induced by inhomogeneous polarization), nor in exploring the single-spin limits of magnetoelastic and/or magnetoelectric coupling in thin films of ferroelectrics rather than single crystals.[21] In contrast to single crystals or epitaxial single layer $PbTiO_3$ thin films, we show that the spins in the Fe^{3+} ions experience a substantial magnetocrystalline anisotropy which rotates with the local polarization texture, as confirmed by first-principles

calculations.

Superlattices of $[(Fe\text{-}PbTiO_3)_{16}/(SrTiO_3)_{16}]_8$ and single layers 50-100 nm Fe-$PbTiO_3$ were synthesized on single-crystalline $DyScO_3$ (001) and $SrTiO_3$ (001) substrates by reflection high-energy electron diffraction (RHEED)-assisted pulsed-laser deposition (Methods section in supplementary and Supplementary Fig. 1). Three-dimensional reciprocal space mapping (RSM) of the superlattice (Fig. 1) about the 002-diffraction condition at 80K and room temperature shows long range satellite peaks around the film peak along the in-plane directions (side lobes, Fig. 1a), corresponding to a vortex ordered phase with a periodicity of ~8 nm on $DyScO_3$ substrate and a skyrmion ordered phase with periodicity of ~8 nm on $SrTiO_3$ substrate. To clarify this diffraction information, we now present real-space imaging results by transmission electron microscopy (TEM). Room temperature vector mapping of the atomic polar displacement ($\boldsymbol{P}_{PD}$) on the cross-sectional HR-STEM image for the superlattice [Fig. 1(b)] is used to probe the local absence of inversion symmetry of the lattice. The vector map of these polar displacements indicates the formation of a long-range array of clockwise (CW) and counterclockwise (CCW) vortex pairs in each Fe-$PbTiO_3$ layer of the superlattice i.e., the continuous rotation of the polarization state within the CW-CCW vortex pairs. The lateral periodicity of this pair is approximately 10 nm which is essentially identical to that observed in RSM studies. This schematic (Fig.1c) also showed the local field and coupling of polarization and the spin in the TiO_6 octahedra changes depending on its position within the vortex. The polarization evolution in the vortex thus provides a platform to impose systematically varying polarization on the Fe-$PbTiO_3$ layer and probe the effects on the S=5/2 Fe^{3+} spins.

EPR is ideal for probing the unpaired spins in the Fe^{3+} ions that are embedded in such a polar vortex. Figure 2 demonstrates angular variations of Fe^{3+} EPR spectra measured at 5 K and magnetic field along the three orthogonal planes associated with the $DyScO_3$ pseudocubic planes: $(010)_{pc}$, $(100)_{pc}$ and $(001)_{pc}$ as shown in Fig. 2a-c. For comparison, the EPR spectra of a single-layer Fe-$PbTiO_3$ thin film with thickness of 100 nm acquired in the (010) plane is shown in Fig. 2d. The low temperature measurements provide spectra with sufficient signal-to-noise ratio for both superlattices and single-layered thin films when the total number of Fe^{3+} spins does not exceed 4×10^{13} spins, consistent with the 1 at.% doping level of the films.

Only one transition is seen at the microwave frequency of 9.4 GHz used in our measurements. It corresponds to the $m_S = 1/2 \leftrightarrow -1/2$ transition within the total spin S = 5/2 multiplet. The angular dependencies are typical for Fe^{3+} located at the Ti^{4+} site with a strong tetragonal distortion of the oxygen octahedron similar to that in bulk $PbTiO_3$ crystals.[21,26,27] The large tetragonal crystal field of the $PbTiO_3$ lattice[28,29] mixes states within the S = 5/2 multiplet; therefore the states involved in the central transition are not pure $m_S = \pm1/2$. This, in turn, leads to a strong dependence of the resonance field as a function of the orientation of the *H*-field with respect to the crystallographic axes. The effective *g*-factor for the transition varies between $g_{eff} \sim 6$ for $H \perp c$ (corresponding to an EPR transition at H_{res} = 1050-1150 Oe) and $g_{eff} \sim 2$ (H_{res} = 3300-3400 Oe) for $H \,//\, c$ (here *c* is the tetragonal axis of $PbTiO_3$, which coincides with the **z** magnetic axis of the Fe^{3+} ion). An explicit expression for g_{eff} and its dependence on the crystal field parameters, calculated in the perturbation limit[30] is presented in the Supplementary Methods section. Thus the *H*-field position of the EPR transition offers us a probe of the local orientation of the *c*-axis and thus the local electric polarization; conversely,

by manipulating the ferroelectric polarization, we have control over the Fe^{3+} spin Hamiltonian.

The measured spectra indicate that Fe-PTO/STO superlattices have components with the *c*-axis direction along all the cubic {100} directions. The corresponding spectral lines from them are indicated in Fig. 2. The most intense spectrum is observed for the spin in the environment of the vortex with *c*-axis orientation along the [001] direction, i.e., along a direction perpendicular to the film plane. Roughly estimated from EPR intensity, the population of these regions is 70-80%. The population of regions with their *c*-axis is oriented away from the [001] direction is ~ 20-30%. However, the actual population of these regions is expected to be bigger as not all Fe^{3+} spins can be properly accounted due to broad spectral lines. As noted previously [22], the marked population of these regions with *c*-axis in the plane of the film reveals, at the nanoscale, a smooth rotation of electric polarization under the influence of depolarization fields and strains at Fe-PTO/STO interfaces. It should be noted that the Fe^{3+} spectrum is very sensitive to the fluctuation of *c*-axis direction especially at angles $\theta = \angle(\mathbf{c},\mathbf{H}) = 15\text{-}20^0$, where the angular variation of the resonance field is the most rapid. The fluctuation of the magnetic axis (and thus the *c*-axis) is reflected in the angular dependence of the linewidth, which is proportional to $dH_r/d\theta$ (where H_r is the resonance field) and has a characteristic maximum at $\theta = 15\text{-}20^0$ (Fig. 3). These data for *c*-type regions (assuming a Gaussian distribution of the deviation angle) were fitted by taking the mean value of the *c*-axis deviation of 2.6^0 for Fe-$PbTiO_3$/$SrTiO_3$ superlattices. For comparison, Fig. 3 also contains data for a $PbTiO_3$ single crystal, where only a negligibly small increase of linewidth can be seen. The *c*-axis fluctuation for *a*-type regions is likely larger since the spectral lines from these regions can be clearly distinguished only around $\theta = 90^0$, where the resonance field is insensitive to *c*-axis fluctuations.

At other angles, i.e., between $\theta = 0^0$ and $\theta = 70^0$, the spectral line is not clearly visible, likely due to strong line-broadening. The observed deviation of the *c*-axis directions from the [001] cubic axis clearly indicates that Fe^{3+} ions undergo shifts along direction perpendicular to the O – Fe – O bond direction (inset of Supplementary figure 2, Fig.1c). Oxygen ions can be shifted as well in the opposite direction as we see only the resultant effect from anion and Fe-ion shifts. Most likely, the anions undergo much larger shifts as Fe^{3+} prefers to be at the center of the oxygen octahedron.[31] This off-center shift in directions perpendicular to the *c*-axis can be easily estimated from the O – Fe – O angle: it is 0.04-0.05 Å. Of course, for oxygen octahedra with Ti^{4+} ions, this off-center shift must be much larger, especially in *a*-type regions. This will lead to the appearance of a dipole moment component along a direction perpendicular to the *c*-axis, i.e. the appearance of the *x* and *y* components of the polarization, thus allowing a rotation of the local polarization. Note that the perpendicular components of the polar displacement determined from EPR data are in a good agreement with those observed in scanning transmission electron microscopy.[24] Finally, the observed Fe^{3+} EPR spectrum in Fe-$PbTiO_3$/$SrTiO_3$ superlattices may also contain contributions from Fe^{3+} ions coupled to an oxygen vacancy, Fe^{3+} - V_O centers, in spite of annealing of films in oxygen atmosphere (details in methods). Isolated Fe^{3+} ions and Fe^{3+} - V_O cannot be distinguished one from the other by measuring only the $m_S = 1/2 \leftrightarrow -1/2$ central transition at 9.4 GHz.[19] However, the presence of oxygen vacancies does not influence the behavior of spectra under influence of electric fields as the Fe^{3+} - V_O dipole is always aligned along the *c*-axis.[28]

The observed tetragonal symmetry of the Fe^{3+} EPR spectrum reflects only the average symmetry over all spins of the Fe^{3+} centers, which in reality are non-tetragonal due to the

presence of non-zero P_x and P_y components of polarization. This will lead to the appearance of rhombic components (*E*-constant in the spin Hamiltonian of a paramagnetic ion, see, for example, spin Hamiltonian in Supplementary) in the crystal field energy landscape. As shown in our EPR data, it originates from ionic shifts along directions perpendicular to *c*-axis. This rhombic term only slightly influences the $m_S = 1/2 \leftrightarrow -1/2$ central transition. It leads to a shift of the *g*-factor on the order of $\approx 24E/D$, where $D \approx 0.6$ cm^{-1} >> *E*. Because the magnetic anisotropy axis continuously rotates along with local polarization, the presence of rhombicity will lead to only spectral line broadening as EPR measures the contribution from all spins thus leaving thus the average tetragonal symmetry along the cubic [100] directions. Due to the line broadening a part of the Fe^{3+} spectrum is not observable; this is reflected in the lower intensity of spectra for the superlattice as compared to the spectra for the single layer film of the same total PTO thickness (Fig. 4). This broadening leads to the lack of observability of the EPR spectrum over a range of magnetic field orientations, as can be seen in the angle dependency in Fig. 2

To understand the effect of the rotating polarization on the electron spins of the Fe-impurities, we calculated the preferential spin axis at each site in a vortex using density functional theory (DFT)[31]. There are practical limitations to performing first-principles calculations directly on $PbTiO_3/SrTiO_3$ superlattices with Fe impurities due to the size of the simulation cell needed to contain the vortices and the need to include spin-orbit coupling effects in calculations. We therefore use the following approximations to make a computationally feasible estimate of the local magnetocrystalline anisotropy at each site. Firstly, we take the atomic structure from second-principles simulations, which we have previously shown to be

comparable to vortex structures obtained from full first-principles simulations.[32] Secondly, we assume that the Fe impurity exactly follows the displacement of the Ti atom that it replaces. This is a reasonable assumption based on our previous work which showed that Fe substitutions for Ti in $PbTiO_3$ follow tetragonal, orthorhombic and rhombohedral distortions when full structure optimization calculations are performed, albeit with a smaller distortion amplitude.[20] Thirdly, we reduce the size of the simulation cell by replicating the local environment around each B-site in a 3x3x3 supercell. This supercell is large enough to contain the charge density associated with the Fe impurity and thus sufficiently represents the crystal field environments of the Fe defect which determines the magnetocrystalline anisotropy energy (MCAE). Moreover this cell size ensures negligible interactions between neighbouring Fe ions. Lastly, the smallest superlattice size necessary to contain the vortices was chosen - 8 unit cells of $PbTiO_3$ on 8 unit cells of $SrTiO_3$ - to limit the number of B-sites in the $PbTiO_3$ layer to 144 (necessitating calculations on 144 supercells of size 3x3x3). This differs from the experimental sample which was 16 unit cells of $PbTiO_3$ on 16 unit cells of $SrTiO_3$ such that the vortex size is a factor of four larger, but should not qualitatively affect our conclusions.

Fig. 5a shows the polarization vector for each unit cell in the $PbTiO_3$ layer of an 8-layer $PbTiO_3$/8-layer $SrTiO_3$ polar vortex and the corresponding spin-easy axes for an isolated Fe^{3+}-dopant at each substitutional Ti-site. These spin axes were extracted from the MCAE surface calculated for an Fe-substitution at each Ti-site individually – i.e., these are the spin properties of a dilute Fe dopant represented at all possible sites in the vortex. The spin easy axes are mainly aligned in the *ab*-plane, and they are canted in this plane due to the varying local polarization environment. The spin axes remain in-plane since the unit cell dimension is longest

in the *c*-direction throughout the vortex structure, such that the B-site displacement within the octahedra is mainly along the *c*-axis, maximizing the orbital angular momentum in the *ab*-plane. The only sites which have the spin-axes out of plane (e.g. I9, J9, P9 in Fig.5a) have maximum B-site displacement along the *a*-axis. The largest MCAE is 280 μeV (site N4) and the smallest is 30 μeV (site D1). There are some sites in the vortex where the MCAE is small despite a large polarization (e.g. site H5); this could occur when the Pb ions cause a large polarization but there is not a large B-site off-centering within the octahedron. Our assumption that the Fe off-centering will exactly follow those of the Ti will systematically overestimate the calculated MCAE magnitude; in our previous work we showed that the Fe off-centering has a smaller magnitude than that of Ti, which will result in a smaller crystal field distortion that dictates the MCAE.[21]

This result of our DFT calculations is in good agreement with Fe^{3+} EPR data which show that the spin easy axis lays in plane perpendicular to the *c*-axis (due to a positive *D* constant, the spin hard axis is oriented along the *c*-axis, as shown in Fig. 5b), and the predicted spin easy axis rotations within this plane are consistent with the spectral line broadening. Moreover, the tetragonal magnetic anisotropy energy calculated from spin Hamiltonian parameters (see section Methods) is ~370 μeV, in reasonable agreement with the DFT calculations, taking into account that the rhombic components of crystal field were not included in the former calculation (their actual value cannot be credibly determined from our spectra, but they likely are non-zero). These rhombic components of the crystal field are directly related to polarization components in the plane normal to the tetragonal *c*-axis and thus will determine the direction of the spin easy axis.

In summary, we present a study into the inherent variation of spin-polarization in ferroelectric vortices and skyrmions of the Fe-doped epitaxial $PbTiO_3/SrTiO_3$ superlattices by a combination of structural and EPR measurements and *ab-initio* calculations. We believe this effect can be significantly enhanced by appropriate design of the host ferroelectric material (e.g., its tetragonality, the chemical species, isotopic purity, *etc*.). From a broader perspective, the wide spectrum of ferroelectric materials, spanning inorganic oxides to polymeric systems (such as PVDF) presents an interesting platform to explore quantum phenomena. We hope this work will stimulate the convergence of the field of quantum computing and spins in ferroelectrics. Going from crystals to epitaxial thin films provides us with explicit pathways to change the intrinsic crystal symmetry and thus change the symmetry of the magnetocrystalline anisotropy from easy plane to easy axis. Finally, we note that although we have used Fe^{3+} as the spin system, the perovskite structure provides us with a multitude of possible spin systems to incorporate, both at the Pb-site as well as the Ti-site. Also, to replace Fe^{3+} to 4d or 5d elements, which will lead to much stronger spin-orbit coupling could enhanced the spin-polarization coupling. In the same vein, although we have used Pb^{2+} as the A-site species, it is perhaps not the most ideal host chemical species (it is not friendly to the environment), although it contributes significantly to the large spontaneous polarization through its 6s-electronic structure. Replacing Pb^{2+} with Ba^{2+} (i.e., going from $PbTiO_3$ to $BaTiO_3$) should likely alleviate this significantly, with the added advantage that there are significantly fewer isotopes for Ba compared to Pb (and thus a lower probability for spin scattering from the nuclear spins).

Acknowledgments The work at UC Berkeley was supported in part by the Center for Probabilistic Spin Logic for Low-Energy Boolean and Non-Boolean Computing (CAPSL), one of the Nanoelectronic Computing Research (nCORE) Centers as task 2759.002, and a Semiconductor Research Corporation (SRC) program sponsored by the NSF through CCF 1739635. Support from the DOE EFRC on Quantum Coherence is gratefully acknowledged. The theory/calculations (KI, SMG) were supported by the Quantum Systems Accelerator, a DOE National Quantum Information Science Center. Computational resources were provided by the National Energy Research Scientific Computing Center and the Molecular Foundry, DOE Office of Science User Facilities supported by the Office of Science, U.S. Department of Energy under Contract No. DE-AC02-05CH11231. The work performed at the Molecular Foundry was supported by the Office of Science, Office of Basic Energy Sciences, of the U.S. Department of Energy under the same contract. V.V.L. thanks the support from the Ministry of Education, Youth and Sports of Czech Republic under project No CZ.02.1.01/0.0/0.0/16_013/0001406. SD gratefully acknowledge a start-up grant from Indian Institute of Science, Bangalore.

Author contributions S.D., W.C.H. and R.R. designed the experiments. S.D. and W.C.H. carried out the synthesis and characterization of the thin films via RHEED-assisted pulsed-laser deposition; W.C.H. and S. D. carried out the X-ray studies of these samples using lab-based X-ray diffraction. W.C.H fabricated the devices. W.C.H., R.C. and V.V.L performed EPR measurements for thin films. W.C.H. and S.D. performed the electric field dependent EPR measurements with R.C.'s assistance. K.I. and S.M.G. performed DFT calculations and theory. R.R., S.M.G., W.C.H., S.D., K.I., and V.V.L. analyzed the data and co-wrote the manuscript. R.R. and S.M.G. supervised the research. All authors contributed to the discussions and

manuscript preparation.

Competing interests The authors declare no competing interests.

REFERENCES

[1] Steane, A. Quantum computing. *Rep. Prog. Phys.* **61**, 117-173, (1998).

[2] Hanson, R. & Awschalom, D. D. Coherent manipulation of single spins in semiconductors. *Nature* **453**, 1043-1049, (2008).

[3] Manipatruni, S. *et al.* Scalable energy-efficient magnetoelectric spin-orbit logic. *Nature* **565**, 35-42, (2019).

[4] Valencia, S. et al, Interface-induced room-temperature multiferroicity in $BaTiO_3$. *Nature Materials* 10, 753 (2011).

[5] Chiba, D.; Fukami, S.; Shimamura, K.; Ishiwata, N.; Kobayashi, K.; Ono, T., Electrical control of the ferromagnetic phase transition in cobalt at room temperature. *Nature Materials* **10,** 853-6 (2011).

[6] Cherifi, R. O.; Ivanovskaya, V.; Phillips, L. C.; Zobelli, A.; Infante, I. C.; Jacquet, E.; Garcia, V.; Fusil, S.; Briddon, P. R.; Guiblin, N.; Mougin, A.; Unal, A. A.; Kronast, F.; Valencia, S.; Dkhil, B.; Barthelemy, A.; Bibes, M., Electric-field control of magnetic order above room temperature. *Nature Materials* **13,** 345-51 (2014).

[7] Yang, S. W.; Peng, R. C.; Jiang, T.; Liu, Y. K.; Feng, L.; Wang, J. J.; Chen, L. Q.; Li, X. G.; Nan, C. W., Non-volatile 180 degrees magnetization reversal by an electric field in multiferroic heterostructures. *Adv Mater* **26** 7091-5 (2014).

[8] Gajek, M. et al, Tunnel junctions with multiferroic barriers. *Nature Materials* **6**, 296–302 (2007).

[9] Heron, J. T.; Bosse, J. L.; He, Q.; Gao, Y.; Trassin, M.; Ye, L.; Clarkson, J. D.; Wang, C.; Liu, J.; Salahuddin, S.; Ralph, D. C.; Schlom, D. G.; Iniguez, J.; Huey, B. D.; Ramesh, R., Deterministic switching of ferromagnetism at room temperature using an electric field. *Nature* **516,** 370-3 (2014).

[10] Fechner, M.; Zahn, P.; Ostanin, S.; Bibes, M.; Mertig, I., Switching magnetization 180º with an electric field. *Phys Rev Lett***. 108,** 197206 (2012).

[11] Boudalis, A. K., Robert, J. & Turek, P. First Demonstration of Magnetoelectric Coupling in a Polynuclear Molecular Nanomagnet: Single-Crystal EPR Studies of $[Fe_3O(O_2CPh)_6(py)_3]ClO_4$ py under Static Electric Fields. *Chemistry* **24**, 14896-14900, (2018).

[12] Liu, J. *et al.* Electric Field Control of Spins in Molecular Magnets. *Phys Rev Lett* **122**, 037202, (2019).

[13] Fittipaldi, M. *et al.* Electric field modulation of magnetic exchange in molecular helices. *Nat Mater* **18**, 329-334, (2019).

[14] Liu, J. et al, Quantum coherent spin–electric control in a molecular nanomagnet at clock transitions. Nature Phys. **17**, 1205-1209 (2021)

[15] Tokura, Y. & Nagaosa, N. Orbital physics in transition-metal oxides. *Science* **288**, 462-468 (2000).

[16] Imada, M., Fujimori, A. & Tokura, Y. Metal-insulator transitions. *Rev. Mod. Phys.* **70**, 1039-1263 (1998).

[17] Monkman, E. J. *et al*. Quantum many-body interactions in digital oxide superlattices. *Nature Mater.* **11**, 855-859 (2012).

[18] Tenne *et al*. Probing nanoscale ferroelectricity by ultraviolet Raman spectroscopy. *Science* **313**, 1614-1616 (2006).

[19] Lee *et al*. Strong polarization enhancement in asymmetric three-component ferroelectric superlattice. *Nature* **433**, 393 (2004).

[20] Chen et al., Advanced Materials, 33, 2000857 (2021)

[21] J. Liu, V. V. Laguta, K. Inzani, W. Huang, S. Das, R. Chatterjee, E. Sheridan, S. M. Griffin, A. Ardavan, and R. Ramesh, *Science Advances* **7**, eabf8103 (2021).

[22] Yadav, A. et al, Observation of polar vortex in oxide superlattices. *Nature* **530**, 198-201 (2016).

[23] Das, S et al, Observation of room temperature polar skyrmion. *Nature* **568**, 368-372 (2019).

[24] Sandhya, S et al, Atomic scale crystal field mapping of polar vortices in oxide superlattices, *Nat. Comms.* **12**, 1-7 (2021)

[25] Warren, W. L., Dimos, D., Pike, G. E., Vanheusden, K. & Ramesh, R. Alignment of defect dipoles in polycrystalline ferroelectrics. *Applied Physics Letters* **67**, 1689-1691, (1995).

[26] Warren, W. L. *et al.* Defect-dipole alignment and tetragonal strain in ferroelectrics. *Journal of Applied Physics* **79**, 9250-9257, (1996).

[27] Muller, K. A. & Berlinger, W. Microscopic probing of order-disorder versus displacive behavior in $BaTiO_3$ by Fe^{3+} EPR. *Phys Rev B Condens Matter* **34**, 6130-6136, (1986).

[28] Laguta, V. V. *et al.* Impurity centers in $PbTiO_3$ single crystals: An electron-spin-resonance analysis. *Physical Review B* **54**, 12353-12360, (1996).

[29] Keeble, D. J. *et al.* Fe^{3+}defect dipole centers in ferroelectric $PbTiO_3$ studied using electron paramagnetic resonance. *Physical Review B* **80**, 014101, (2009).

[30] von Waldkirch, T., Müller, K. A. & Berlinger, W. Analysis of the Fe^{3+}-V_O Center in the Tetragonal Phase of $SrTiO_3$. *Physical Review B* 5, 4324-4334, (1972).

[31] H. Mestric et al., Iron-oxygen vacancy defect centers in $PbTiO_3$: Newwman superposition model analysis and density functional calculations Phys. Rev. B 71, 134109 (2005)

[32] Aguado-Puente, P., & Junquera, J. (2012). Structural and energetic properties of domains in $PbTiO_3$/$SrTiO_3$ superlattices from first principles. Physical Review B, 85(18), 184105.

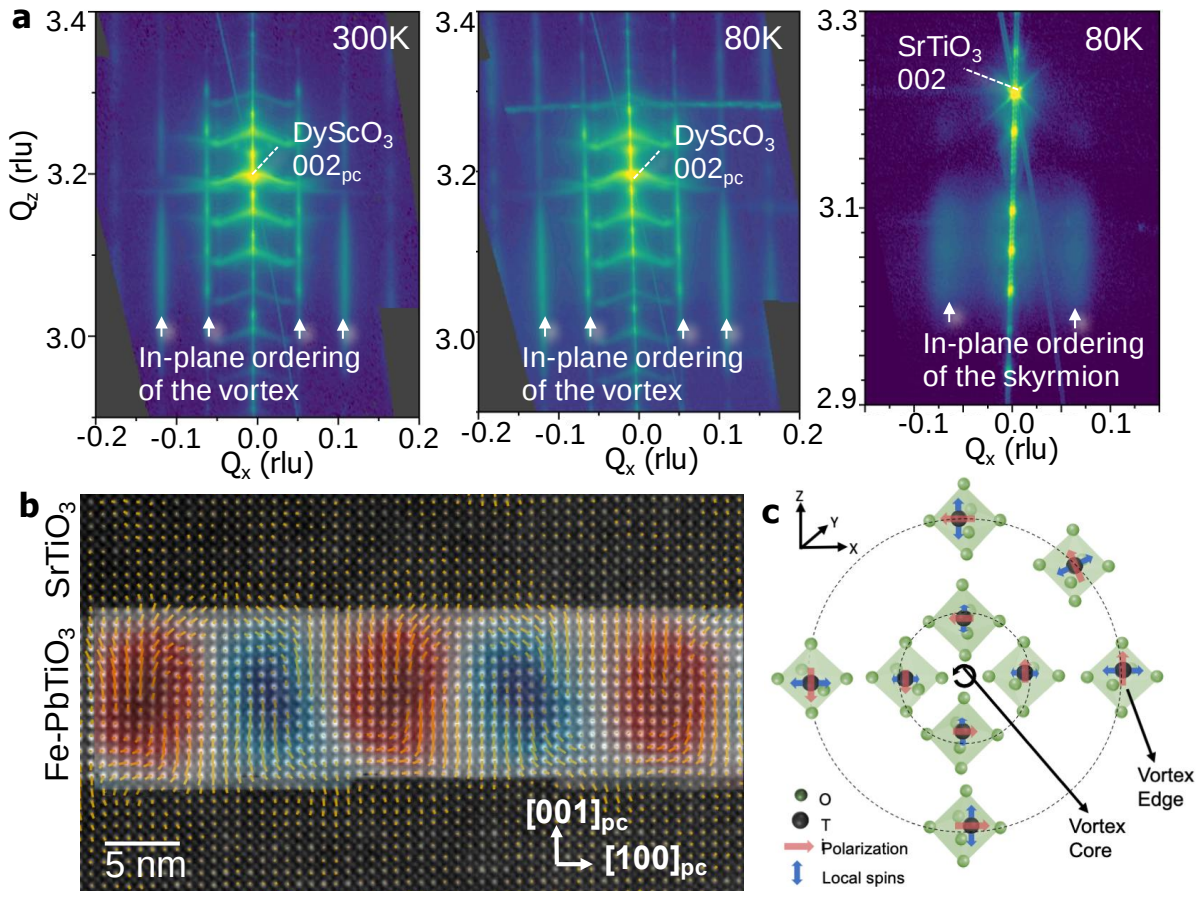

Figure 1| Structural characterization of Fe-$PbTiO_3$/$SrTiO_3$ superlattice. Reciprocal space mapping (RSM) studies for the $[(\text{Fe-PbTiO}_3)_{16}/(\text{SrTiO}_3)_{16}]_8$ superlattice about the 002_{pc}-diffraction peak of: **a,** $DyScO_3$ substrate at 300K (left), at 80K (middle) revealing satellite peaks along the in-plane (Q_x) direction, corresponding to the ordering of the vortex pairs and $SrTiO_3$ substrate at 80K (right) revealing satellite peaks along the in-plane (Q_x) direction, corresponding to the ordering of the skyrmiron. **b,** Cross-sectional HR-STEM image with mapping of the titanium-ion displacement vectors ($\boldsymbol{P}_{PD}$, indicated by orange arrows) for the superlattice at 300K, revealing a quasi-ordered array of left- and right-handed vortices in pairs in the Fe-$PbTiO_3$ layer. **c,** schematic representing the rotation of TiO_6 octahedra including coupled between polarization (red arrow) and local spin (blue arrow) within one vortex domain.

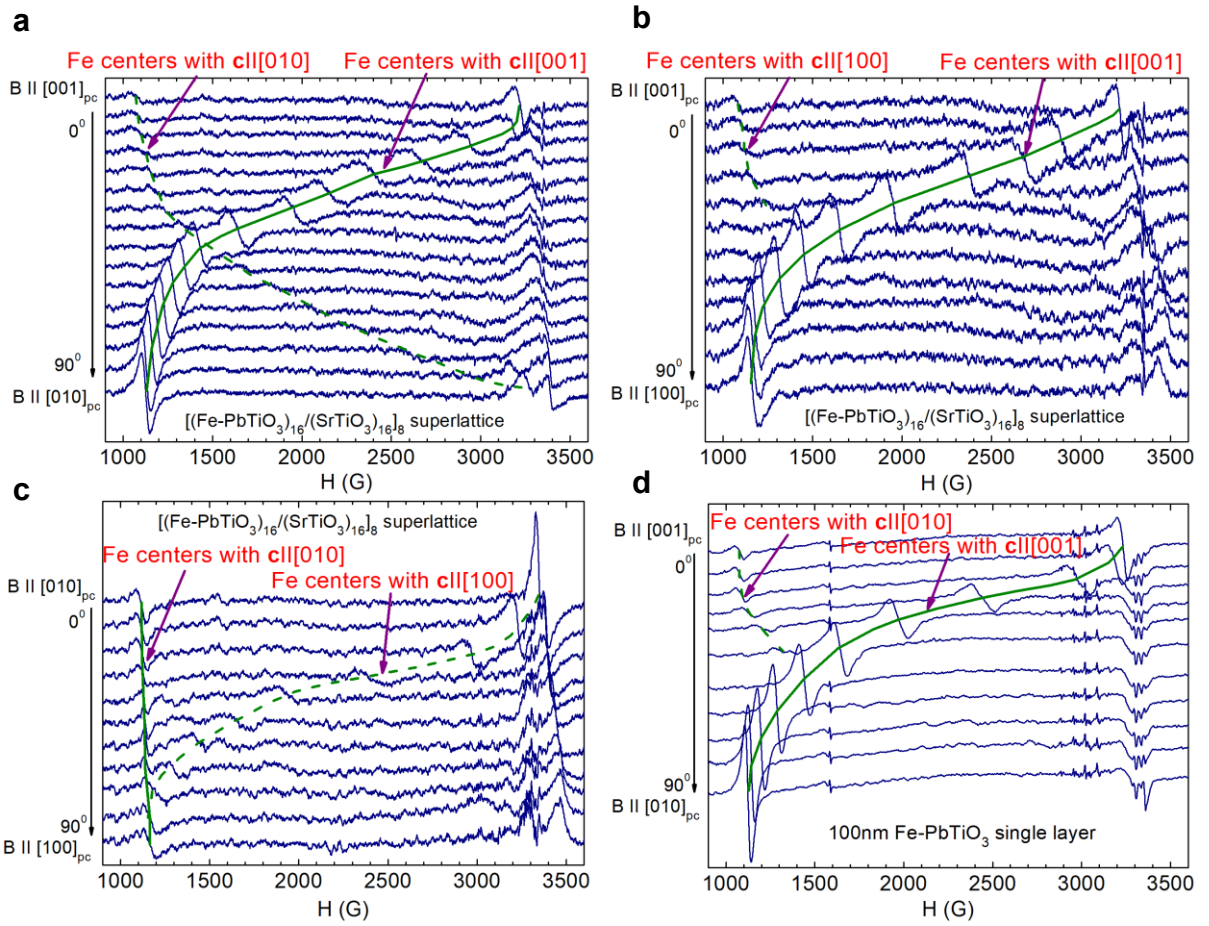

Figure 2| Angular variations of the Fe^{3+} Electron paramagnetic resonance spectra measured in $[(Fe\text{-}PbTiO_3)_{16}/(SrTiO_3)_{16}]_8$ superlattice on $DyScO_3$ substrate at 5 K a, at magnetic field rotation in $(100)_{pc}$ plane, **b,** at magnetic field rotation in $(010)_{pc}$ plane, and **c,** at magnetic field rotation in $(001)_{pc}$ plane. **d,** For comparison, angular dependence of the Fe^{3+} spectra measured in Fe-$PbTiO_3$ single layer. A small shift of resonance field for Fe centers with **c** || [010] in figure **c** is caused by the influence of $DyScO_3$ induced magnetization, the value of which depends on *H*-field direction.

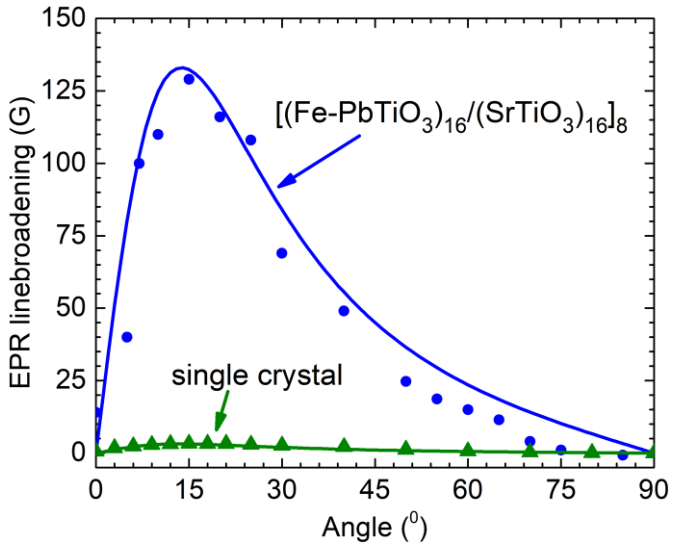

Figure 3| Angular dependence of Fe^{3+} EPR line boadening for the magnetic field rotation in $(100)_{pc}$ plane for $[(Fe\text{-}PbTiO_3)_{16}/(SrTiO_3)_{16}]_8$ superlattice and $Fe\text{-}PbTiO_3$ single crystal. The variation of the magnetic axis (and thus *c*-axis), which is proportional to $dH_r/d\theta$, is reflected in the line broadening, and is maximum at θ=15-20^0. Solid lines are the theoretical fit.

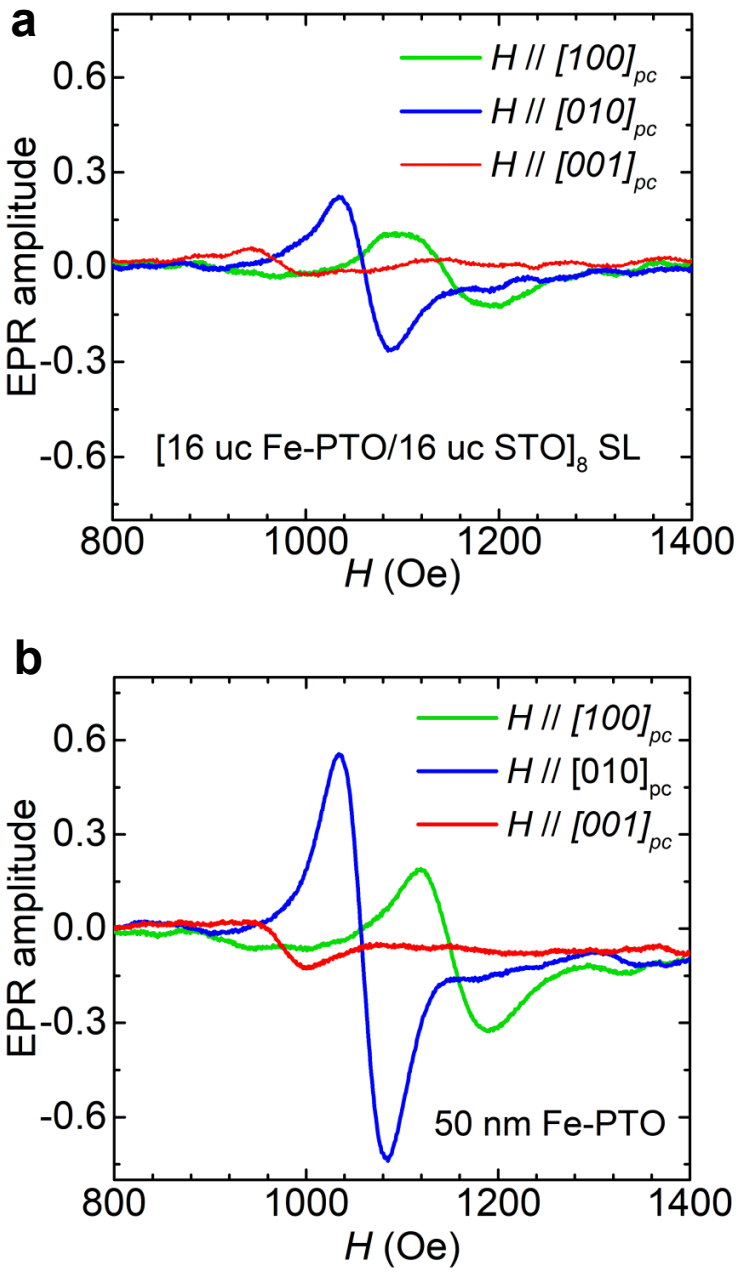

Figure 4| EPR anisotropy in Fe-$PbTiO_3$/$SrTiO_3$ superlattice and 50nm Fe-$PbTiO_3$ thin films. a, EPR spectra at 5 K with *H* along $[100]_{pc}$, $[010]_{pc}$ and $[001]_{pc}$ axis of the $[(Fe\text{-}PbTiO_3)_{16}/(SrTiO_3)_{16}]_8$ superlattice which has CW-CCW vortices. **b,** 50nm Fe-$PbTiO_3$ single layer. A small shift of resonance field for different directions of *H*-field is caused by the influence of $DyScO_3$ induced magnetization, the value of which depends on *H*-field direction.

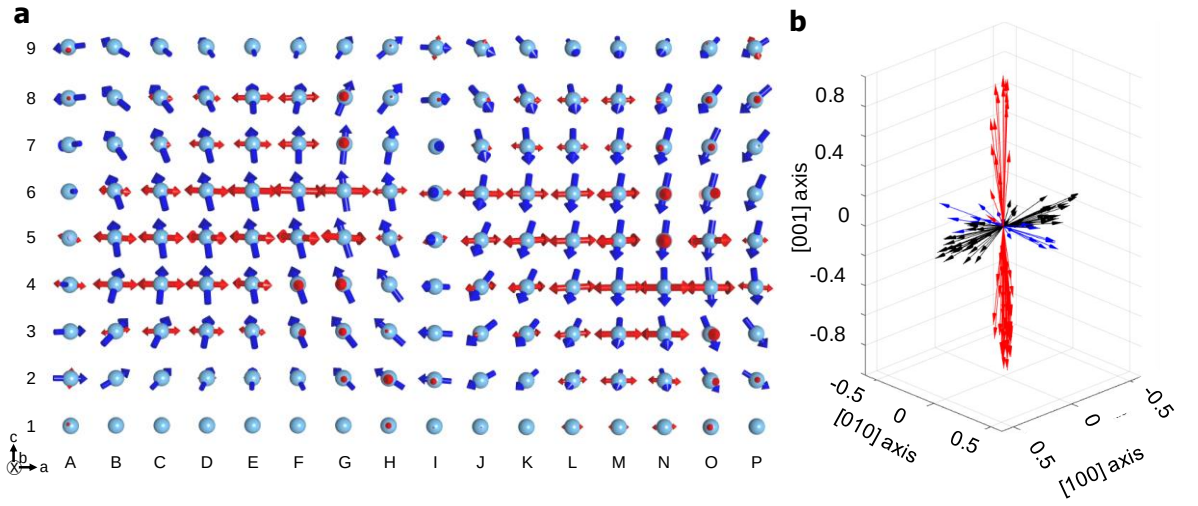

Figure 5| Interplay of lattice polarization and Fe^{3+}-dopant spin axis on each possible vortex site. a, $PbTiO_3$ layer of an 8-layer $PbTiO_3$/8-layer $SrTiO_3$ polar vortex structure showing only the Ti atoms (pale blue spheres) of the $PbTiO_3$ layer. Blue arrows indicate the electronic polarization vector calculated at each $PbTiO_3$ unit cell. Red arrows show the spin easy axes for an isolated Fe^{3+}-dopant calculated on each Ti-site individually, and these are scaled to the magnitude of the magnetocrystalline anisotropy energy. **b,** Local magnetic anisotropy for all possible vortex sites. The arrows show the orientations for the local *D* anisotropy for all possible Fe^{3+} calculated by DFT. The length of the arrow is scaled proportional to the magnitude of *D*. The majority of the principal magnetic anisotropy axes, i.e. *c*-axis, are found to be close to the [001] axis, as indicated by the red arrows. For the rest of Fe^{3+} in the *a*-type region, the magnetic anisotropy axes prefer to align close to the [100] axis (black arrows) over the [010] axis (blue arrows).

TOC Graphic